2280–2289 Nucleic Acids Research, 2002, Vol. 30, No. 11

Bacillus subtilis bacteriophage SPP1 hexameric DNA helicase, G*40*P, interacts with forked DNA

Silvia Ayora[1,2], Frank Weise[1], Pablo Mesa[1], Andrzej Stasiak[3] and Juan C. Alonso[1,*]

[1]Departamento de Biotecnología Microbiana, Centro Nacional de Biotecnología, C.S.I.C., Campus de la Universidad Autónoma de Madrid, Cantoblanco, E-28049 Madrid, Spain, [2]Departamento de Biología Molecular, Universidad Autónoma de Madrid, Cantoblanco, E-28049 Madrid, Spain and [3]Laboratoire d'Analyse Ultrastructurale, Bâtiment de Biologie, Université de Lausanne, CH-1015 Lausanne-Dorigny, Switzerland

Received March 22, 2002; Revised and Accepted April 3, 2002

ABSTRACT

SPP1-encoded replicative DNA helicase gene *40* product (G*40*P) is an essential product for phage replication. Hexameric G*40*P, in the presence of AMP-PNP, preferentially binds unstructured single-stranded (ss)DNA in a sequence-independent manner. The efficiency of ssDNA binding, nucleotide hydrolysis and the unwinding activity of G*40*P are affected in a different manner by different nucleotide cofactors. Nuclease protection studies suggest that G*40*P protects the 5′ tail of a forked molecule, and the duplex region at the junction against exonuclease attack. G*40*P does not protect the 3′ tail of a forked molecule from exonuclease attack. By using electron microscopy we confirm that the ssDNA transverses the centre of the hexameric ring. Our results show that hexameric G*40*P DNA helicase encircles the 5′ tail, interacts with the duplex DNA at the ss–double-stranded DNA junction and excludes the 3′ tail of the forked DNA.

INTRODUCTION

Initiation of *Bacillus subtilis* bacteriophage SPP1 DNA replication, which is probably the simplest DNA replication system described so far, requires phage-encoded gene *36*, *38*, *39* and *40* products (G*36*P, G*38*P, G*39*P and G*40*P), as well as the host-encoded DNA primase (DnaG), DNA polymerase III (DNA PolIII), DNA topoisomerases and DNA ligase proteins (1–3). Multiple copies of G*38*P bound to its cognate sites (*ori*L and *ori*R) induce local unwinding of the adjacent A + T-rich sequence leading to open complex formation (2,3). The single-stranded binding protein, G*36*P, binds to the single-stranded (ss)DNA at the open complex. G*39*P, upon interaction with *ori*L-bound G38P, loads the G*40*P-ATP replicative helicase onto the SPP1 replication origin (2,3). Then, G*40*P-ATP bound at the open complex directs the loading of DnaG (4).

G*40*P, which is a member of the bacterial DnaB family of DNA helicases, is a homohexamer that couples the hydrolysis of nucleoside triphosphates to nucleic acid unwinding with a 5′ → 3′ polarity (3,5, reviewed in 6). However, how DNA can be unwound and how NTP hydrolysis is coupled to movement and base pair separation are still open questions in this family of helicases, especially due to the lack of structural studies of DnaB-like helicases complexed with DNA, which can provide clues into the steps along the catalytic cycle of these enzymes. Electron microscopic studies indicate that DnaB and G*40*P exist in an equilibrium of two conformational states [with a 6-fold (C_6) and a 3-fold (C_3) symmetry] (5,7,8), but the significance of both states remains unknown.

In this report we explored some properties of the hexameric G*40*P replicative DNA helicase in order to know how the protein interacts with forked DNA. G*40*P shows a nucleotide hydrolysis activity that is modulated by the presence of different cofactors, and ATP is the preferred nucleotide for unwinding. ssDNA, which traverses the centre of the hexameric ring, forms a stable complex with G*40*P in the presence of a non-hydrolysable nucleotide cofactor, and the binding is modulated by an adjacent double-stranded (ds)DNA region. Nuclease protection studies suggest that, in the presence of a non-hydrolysable ATP analogue, hexameric G*40*P binds to substrates resembling a replication fork, protecting only the 5′ tail of the forked structure. It may interact with the dsDNA without introducing a major distortion of the DNA structure at the junction region.

MATERIALS AND METHODS

Bacterial strains, plasmids and bacteriophages

The *Escherichia coli* strains JM103 (9) and BL21DE3 (10) were used. Plasmids pBT323 (1) and pLysS (10) were described previously. The replicative form (RF) and viral M13mp18 (9) were used.

Enzymes and reagents

The protease inhibitor phenylmethylsulfonyl fluoride (PMSF) was from Roche Diagnostics and isopropyl-β-D-thiogalactopyranoside (IPTG) was from Calbiochem. DEAE-Sepharose, Q-Sepharose, Sephadex G-100 and Superose 12 were from Pharmacia, and phosphocellulose was from Whatman. Exonuclease III (*Exo*III), exonuclease VI (*Exo*VI) and exonuclease VII (*Exo*VII) were from USB.

*To whom correspondence should be addressed. Tel: +34 91 585 4546; Fax: +34 91 585 4506; Email: jcalonso@cnb.uam.es
Present address:
Frank Weise, Max-Planck-Institut für Biologie, Corrensstrasse 38, D-72076 Tübingen, Germany

M13mp18 RF (dsDNA) and viral ssDNA were prepared as described (11). The labelling of DNA ends was performed as described (11). Labelled oligonucleotide with the appropriate length was gel purified. The linearised and labelled M13mp18 ssDNA was separated from the oligonucleotides generated by heating and further purification through a Sephadex G-100 column. The DNA helicase substrate, consisting of a 50-nt long ssDNA segment, of which 30 nt are complementary to viral M13mp18 at position 6230–6259 and the remaining 20 nt are unpaired (3′-tail DNA), has been reported previously (12).

The sequence of the oligonucleotides used in the binding studies was: 51 nt (5′-ATCGATGTCTCTCTAGACAGCACGA-GCCCTAACGCCAGAATTCGGCAGCGT-3′); 50 nt (5′-AGA-GGATCCCCGGGTACCGAGCTCGAATTCCATTAGTAC-CAGTATCGACA-3′); 21 nt (5′-GACAATATTAGTTTTGT-TATC-3′); 18 nt (5′-GGCCTTCCTGTAGCCAGC-3′); 16 nt (5′-AAGAAATCGAATCGGA-3′). The 39/16 double-arm substrate consists of a 39-bp duplex and a double arm with 16-nt long poly(dA) ssDNA segments (forked molecule), it is made by annealing 55-nt top (5′-GCTTGCATGCCTGCAGG-TCGACTCTAGAGGATCCCCGGGAAAAAAAAAAAAAA-AAA-3′) and 55-nt bottom (5′-AAAAAAAAAAAAAAAA-CCCGGGGATCCTCTAGAGTCGACCTGCAGGCATGCA-AGC-3′). The 39/25 forked molecule is similar to 39/16, but both ssDNA arms consist of a 25 poly(dA)-nt segment instead of a 16 poly(dA)-nt segment. The 39/16 or 39/25 5′ single-arm substrates were made by annealing a 39-nt top (5′-GCTTG-CATGCCTGCAGGTCGACTCTAGAGGATCCCCGGG-3′) with the complementary 55- or 64-nt bottom oligonucleotides, to generate a 39-bp duplex and a 5′ single-arm fork containing 16- or 25 poly(dA)-nt, respectively. The 39/16 or 39/25 3′ single-arm substrates were made by annealing a 39-nt bottom (5′-CCCGGGGATCCTCTAGAGTCGACCGCAGGCATGC-AAGC-3′) with the complementary 55- or 64-nt top oligo-nucleotides, to generate a 39-bp duplex and a 3′ single-arm fork containing 16- and 25 poly(dA)-nt, respectively. The 39-bp duplex substrate was made by annealing oligonucleotides 39-nt top and 39-nt bottom, and gel purified.

The cold dNTPs, rNTPs, ATPγS, AMP-PNP, the [^{32}P]dNTPs (3000 Ci/mmol) and [^{32}P]rNTPs (3000 Ci/mmol) and poly(dA), poly(dC) and poly(dI)(dC) were purchased from Roche Diagnostics, Amersham Corp. and Sigma Chemical Co., respectively.

Protein purification

G*40*P was purified from *E.coli* BL21(DE3) plysS cells expressing the protein from plasmid pBT323 as follows: the cell paste was resuspended in buffer A [50 mM Tris–HCl pH 7.5, 10 mM $MgCl_2$, 0.5 mM PMSF, 5% (v/v) glycerol] containing 100 mM NaCl and lysed by ultrasonication (20 pulses of 10 s) at 100 W. The cell debris and the DNA were removed by polyethylenimine precipitation. G*40*P was precipitated by addition of solid ammonium sulfate to 60% saturation. The precipitated protein was resuspended in buffer A, dialysed and loaded onto a DEAE-Sepharose column equilibrated with buffer A containing 25 mM NaCl. G*40*P was eluted using a salt gradient, from 100 to 140 mM NaCl in buffer A. G*40*P was loaded onto a Q-Sepharose column, and eluted from the column by a gradient from 120 to 250 mM NaCl in buffer A. G*40*P purified and stored in the presence of Mg^{2+} elutes predominantly with an apparent molecular mass of ~300 kDa, whereas the purification in the absence of the metal ion renders a mixed population of ~80% hexamers, and two minor forms of ~4% of dodecamers and ~16% of monomers. Unless stated otherwise, we are characterising the activity of hexameric G*40*P.

Analysis of the first 10 N-terminal residues of pure G*40*P was in full agreement with the amino acid sequence deduced from the nucleotide sequence of gene *40*. The protein concentration was determined by UV absorbance, using the molar extinction coefficient at 280 nm of 48 970 M^{-1} cm^{-1} as described previously (13) and is expressed in moles of hexamers.

ATPase activity measurement

Standard reactions were incubated for 10 min at 37°C in buffer B [50 mM Tris–HCl pH 7.5, 5 % (v/v) glycerol, 50 µg/ml BSA, 8 mM $MgCl_2$, 1 mM DTT, 50 mM NaCl] with 10 nM of G*40*P in a volume of 25 µl. The ATP concentration used was 1 mM, containing 10 nM of [γ-^{32}P]ATP (1*:100 000). The effector ssDNA used is indicated in each experiment. ATPase activity was determined by measuring the amount of phosphate set free upon hydrolysis as described previously (12).

dNTP or rNTP hydrolysis reactions (25 µl) were performed using a constant amount of 150 µM poly$(dT)_{30}$ and G*40*P (10 nM) and increasing amounts of dNTP (with a constant ratio of 1*:100 000) or rNTP during 10 min at 37°C in buffer B. Products were separated by chromatography on polyethylenimine-cellulose as described previously (14), and the formation of [γ-^{32}P]dNDP or [α-^{32}P]rNDP quantified by using the Molecular Imager (MI) and Molecular Analyst (MA) software package version 2.1 (Bio-Rad). All reactions were performed in duplicate.

Helicase activity measurement

The reaction was incubated for 15 min at 30°C in buffer B containing 2 mM of the different dNTPs or rNTPs with 10 nM of G*40*P in a 20 µl volume as described previously (4). The reaction was stopped by addition of 5 µl of stopping solution [100 mM EDTA, 2% (w/v) SDS in DNA loading buffer] and subsequently separated using a 10% (w/v) non-denaturing polyacryamide gel electrophoresis (ndPAGE). Gels were run and dried prior to autoradiography. The substrate and resulting product were quantified by using the MI and MA software package as described above.

Measurements of G*40*P–DNA complexes

G*40*P–DNA complexes were measured by electrophoretic mobility shift assay (EMSA) as described previously (3).

γ-^{32}P-labelled substrate (dsDNA, ssDNA segments or single- or double-arm molecules) (2 nM) was incubated with increasing concentrations of G*40*P in buffer B containing 1 or 3 mM AMP-PNP or 2 mM of the different NTPs or dNTPs during 10 min at 37°C. The protein–DNA complexes were separated on 8% (w/v) ndPAGE in buffer Tris–glycine pH 8.5 (25 mM Tris, 300 mM glycine and 2 mM $MgCl_2$) containing 20 µM of AMP-PNP or the corresponding NTP or dNTP both, in the gel and buffer, as described previously (3).

Exonuclease protection assays

The protection of a forked molecule by G*40*P (12.5 or 25 nM), in the presence or the absence of 1 mM AMP-PNP, against

exonuclease attack was measured as described previously (15). The 39/16 or 39/25 [γ-^{32}P]-forked substrate, labelled at the 5′ end (top strand), or 39/16 or 39/25 [α-^{32}P]-forked substrate labelled at the 3′ end (bottom strand) were incubated with increasing concentrations of G*40*P in buffer B with or without 1 mM AMP-PNP, during 15 min at 20°C in a volume of 15 µl. *Exo*VII (0.2 U) was then added and the incubation was continued for another 15 min. The reaction was stopped by addition of 10 µl of formamide solution containing 20 mM EDTA, heated for 5 min at 90°C and the products were separated using 10% (w/v) denaturing (d)PAGE run in TBE. The gels were dried, analysed by autoradiography and quantified as described above. [γ-^{32}P]poly(dA) was used as a molecular weight marker.

The 39/16 or 39/25 [γ-^{32}P]-forked substrate, labelled at the 5′ end (bottom strand), was incubated with increasing concentrations of G*40*P in buffer B with or without 1 mM AMP-PNP, during 15 min at 20°C in a volume of 15 µl. *Exo*III (1 U) was then added and the incubation was continued for another 15 min. The reaction was stopped as indicated for the *Exo*VII assays and the products were separated using 15% (w/v) dPAGE run in TBE.

The 39/16 or 39/25 [α-^{32}P]-forked substrate, labelled at the 3′ end (top strand), was incubated with increasing concentrations of G*40*P in buffer B with or without AMP-PNP, during 15 min at 20°C in a volume of 15 µl. *Exo*VI (1 U) was then added and the incubation was continued for another 15 min. The reaction was stopped and the products were separated and quantified as indicated for the *Exo*III assays.

$KMnO_4$ footprinting assay

The protection of a forked molecule by G*40*P (12.5 or 25 nM) against $KMnO_4$ attack, in the presence or the absence of 1 mM AMP-PNP, was measured as described previously (11). The 39/16 or 39/25 [γ-^{32}P]-forked substrate, labelled at the 5′-end (top or bottom strand), was incubated with increasing concentrations of G*40*P in buffer B with or without AMP-PNP, during 15 min at 20°C in a volume of 15 µl. The samples were then treated with 1 mM $KMnO_4$ for 30 s at 37°C, the DNA was precipitated in presence of 1 µg of tRNA and cleaved with piperidine. The samples were separated using 15% (w/v) dPAGE run in TBE, and the gels dried and analysed by autoradiography.

Electron microscopy

Viral M13mp18 (0.2 nM) was incubated in buffer C [20 mM Triethanolamine–HCl pH 7.0, 8 mM magnesium acetate, 50 mM NaCl, 1 mM AMP-PNP, glycerol 8% (v/v)] with G*40*P (50 nM) for 15 min at 37°C in a 10 µl reaction. Complexes were then fixed with 0.15% (w/v) glutaraldehyde and negative stained with uranyl acetate (16).

RESULTS AND DISCUSSION

The ATPase activity of G*40*P is modulated by the presence of different effectors

G*40*P purified from *E.coli* cells was >99% pure as judged by SDS–PAGE followed by Coomassie Blue staining and quantitative sequence analysis (data not shown). Purified G*40*P is free of the *E.coli* DnaB DNA helicase. The separation of G*40*P from DnaB was achieved by a DEAE chromatographic step. G*40*P elutes at ~100–140 mM NaCl, whereas DnaB elutes at 300–400 mM NaCl (data not shown).

The effect of different DNA substrates on G*40*P NTP hydrolysis was analysed. G*40*P was able to hydrolyse ATP to ADP and P_i, and this activity was stimulated up to 5-fold in the presence of artificial ssDNA substrates such as poly(dA), poly(dC) (Fig. 1A) or unstructured 21-nt ssDNA (see below), whereas the stimulation of the ATPase activity was only increased ~3-fold when the ssDNA substrate has a self-annealing potential (e.g. viral M13mp18 ssDNA), or when dsDNA and RNA were used (Fig. 1A–C).

The kinetics of ATP hydrolysis K_m values of G*40*P for ATP in the presence or the absence of poly(dT)$_{30}$ was analysed. In the absence of ssDNA, the ATPase activity increased to reach a plateau at very low ATP concentrations and then decreased slightly at higher ATP concentrations. In the presence of ssDNA, the ATPase activity increased with increasing amounts of ATP up to 0.4–0.8 mM and then decreased at higher ATP concentrations (Fig. 1D). In the presence of 0.4 mM ATP the presence of ssDNA increased ATP hydrolysis up to 5-fold. Michaelis–Menten kinetics has been observed for *E.coli* DnaB, or T7 gp4 helicase (reviewed in 6), but increasing concentrations of ATP have been shown to inhibit the ATPase activity of the only two replicative helicases of Gram-positive bacteria characterised so far, namely *Bacillus stearothermophilus* DnaB (17) and G*40*P (Fig. 1D).

ATP hydrolysis occurs in the presence of Mg^{2+}, to a lesser extent in presence of Mn^{2+}, and Ca^{2+}, but ATP hydrolysis drops to background levels in the presence of Ni^{2+} or Zn^{2+}, or when EDTA was added (Fig. 1E).

The activity of G*40*P is modulated by the different nucleotide cofactors

Although most hexameric helicases do not show a strict nucleotide preference and specificity, as they hydrolyse a number of rNTPs or dNTPs (reviewed in 6,18,19), their nucleotide requirements for the DNA unwinding activity may be more strict (6,18,19), and a comparison of the effect of nucleotides on the three activities that hexameric helicases show has not been done yet. Therefore, the effect of nucleotides on G*40*P NTP hydrolysis, ssDNA binding and DNA unwinding activity was examined. The NTPase activity of G*40*P (10 nM) in the presence of poly(dT)$_{30}$ and increasing concentrations of NTPs was measured. The G*40*P NTPase activity increased with increasing amounts of NTP up to 0.4–0.8 mM and then decreased at higher NTP concentrations (Fig. 2A). G*40*P hydrolyses ATP (at 0.5 mM) with highest efficiency, and the rate of hydrolysis of the other NTPs (at 0.5 mM NTP) is 76 (GTP), 70 (CTP) and 69% (UTP) of the rate of ATP hydrolysis (Fig. 2A).

The apparent binding constant (K_{app}) of G*40*P for a naked 50-nt ssDNA segment observed in the presence of 2 mM CTP was 120 nM. The G*40*P binding affinity to a 50-nt ssDNA was reduced 2.5-, 3- and 5-fold in the presence of ATP, GTP and UTP, respectively (Fig. 2B).

To test the DNA helicase activity of G*40*P (10 nM) in the presence of the dNTPs or rNTPs, M13mp18 ssDNA annealed to a 30-nt segment with a 20-nt non-complementary tail (3′-tailed substrate) was incubated with G*40*P and, after deproteinisation, the unwound products were visualised by 10% ndPAGE. G*40*P

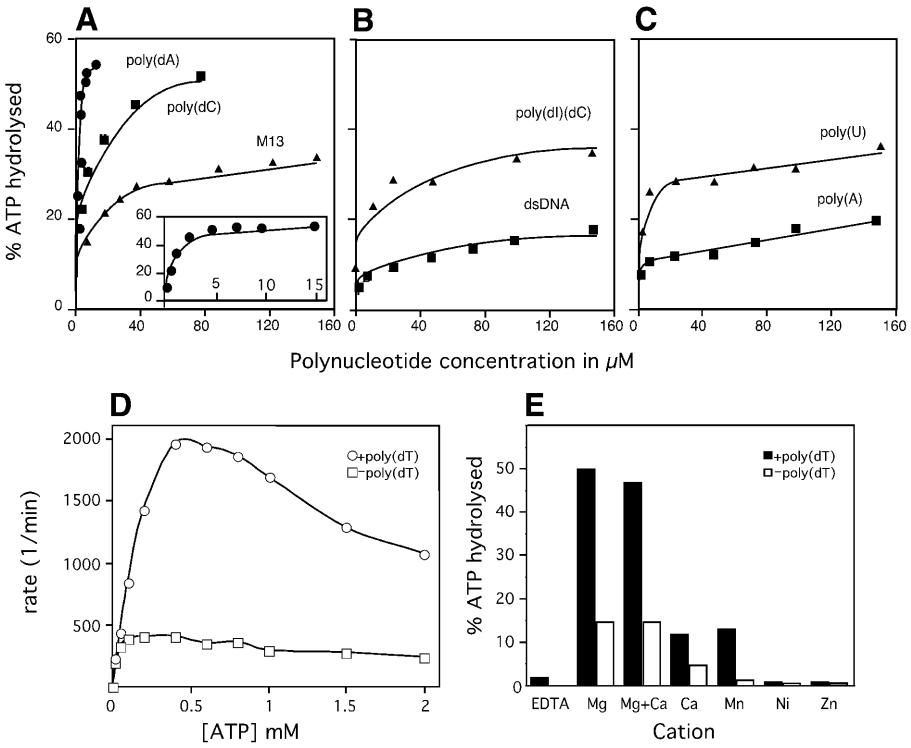

Figure 1. ATPase activity of G*40*P. (**A**, **B** and **C**) The effect of polynucleotide effector concentration on G*40*P ATPase activity is shown. Reactions were as described in the Materials and Methods. ATPase activity of G*40*P is presented as turnover in percent versus concentration of effector nucleotides. (A) ssDNA as effector. The results for poly(dA) are shown enlarged in the small window; (B and C) dsDNA and RNA as effector, respectively. (**D**) ATPase activity in the presence (circles) and absence (squares) of ssDNA as a function of ATP concentration. (**E**) Effect of different cations on the ATPase activity of G*40*P. Filled squares or bars denote results in the presence of ssDNA, and empty squares or bars indicate results in absence of ssDNA.

preferentially unwinds the 50-nt ssDNA segment in the presence of ATP after 15 min of incubation. When the ATP was replaced by GTP, UTP or CTP, under the same conditions, 62, 20 and 42% of the unwinding observed with ATP, respectively, was observed (Fig. 2C). The unwinding activity of G*40*P was not observed in the presence of the four dNTPs. It is probable, therefore, that although G*40*P is able to hydrolyse the four rNTPs (at low NTP concentrations) with similar efficiency, only CTP, GTP and ATP are optimal for binding and hydrolysis, but the unwinding activity is maximal only with ATP, and with GTP to a lesser extent.

G*40*P hydrolyses ATP and GTP binds ssDNA with higher efficiency in the presence of CTP, but unwinds DNA preferentially in the presence of ATP and GTP. *Escherichia coli* DnaB can bind and hydrolyse all rNTPs with similar affinity and efficiency (20), whereas T4 gp41 and T7 gp4 show some preference for purines. T4 gp41 hydrolyses GTP, dGTP, ATP and dATP, but only ATP and GTP support helicase activity (21,22), and T7 gp4 hydrolyses ATP, dATP, dTTP and dGTP, but unwinds DNA in the presence of dTTP, and to some extent with dATP and ATP (23,24).

G*40*P preferentially binds unstructured ssDNA

Previously, the K_{app} of G*40*P for naked linear viral [α-^{32}P]M13mp18 ssDNA or M13mp18 dsDNA, in the presence or absence of saturating amounts of ATP or its poorly hydrolysable analogue (AMP-PNP), was determined by filter binding assay following the amount of complex formation as a function of G*40*P concentration (25). The affinity of G*40*P for dsDNA was shown to be independent of nucleotide and ~20-fold lower than for ssDNA (25). To measure the specificity of binding, a series of unrelated short [γ-^{32}P]ssDNA segments (2 nM) have been used in EMSA in the presence or the absence of a nucleotide cofactor. In the absence of a nucleotide cofactor, the K_{app} of G*40*P for a 51-nt ssDNA was estimated to be ~990 nM, and upon addition of ATP, binding of G*40*P to ssDNA is increased ~3.3-fold (Fig. 3A). When ATP was replaced by non-hydrolysable ATP analogues (1 mM AMP-PNP or ATPγS) the affinity of G*40*P for ssDNA increased ~25-fold (K_{app} ~12 nM) (Fig. 3A). It is probable, therefore, that in the presence of ATP G*40*P binds and releases the ssDNA substrate, whereas in the presence of AMP-PNP stable binding to ssDNA is mainly observed (Fig. 3A). Similar results were obtained when an unrelated 50-nt long ssDNA segment or M13 viral ssDNA (25) were used.

The affinity of G*40*P for a series of unrelated short DNA segments (16–21-nt ssDNA) with no potential DNA pairing is greatly enhanced (G*40*P–ssDNA complex with a K_{app} of ~1.5 nM) when compared with the affinity to the 51- or 50-nt ssDNA segments (G*40*P–ssDNA complex, K_{app} ~13 nM) (Fig. 3A). However, when we used a 55-nt segment consisting of 39 nt of random sequence with low self-annealing potential followed by a poly(dA) 16 nt long, we observed that G*40*P binds to it with similar affinity as to the 16-nt long molecule (see below). These results suggest that G*40*P preferentially binds to unstructured ssDNA and in a sequence-independent manner.

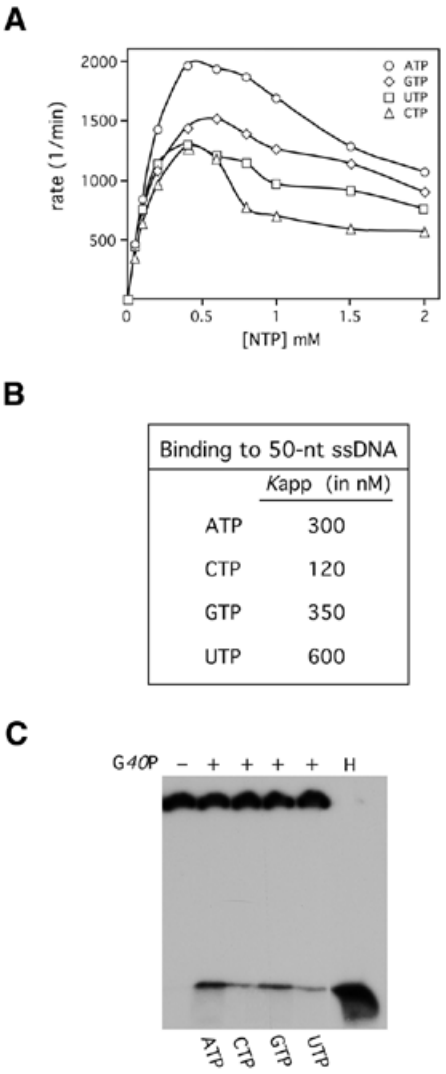

Figure 2. Effect of ribonucleotides on the G*40*P activities. (**A**) NTPase activity of G*40*P in the presence of ssDNA as a function of NTP concentration. (**B**) K_{app} of G*40*P for a 50-nt ssDNA in the presence of 2 mM NTP. (**C**) DNA unwinding activity of G*40*P in the presence of the 2 mM NTP. The symbols + and – denote the presence or absence of G*40*P. H denotes heated susbtrate. The data represent the average of three independent experiments. Experimental details are described in the Materials and Methods.

Previously, it has been shown that the DnaB enzyme binds ~20 ± 3-nt ssDNA that were predicted to be inside the central hole of the hexameric helicase (26). The DnaB binding site is bipartite with ~10-nt ssDNA defining the strong binding site to the C-terminal part and ~10-nt ssDNA a weak binding to the N-terminal half of the enzyme (27). To learn how many G*40*P hexamers bind to a ssDNA segment, a 21- or a 51-nt ssDNA (3 nM) segment was incubated with increasing amounts of G*40*P and the protein–ssDNA complexes separated by ndPAGE. G*40*P forms one type of complex (I) with the 21-nt ssDNA segment even at high G*40*P protein concentrations, but two types of complexes (I and II) were observed with the 51-nt ssDNA segment (Fig. 3B). Under equilibrium conditions, in the presence of AMP-PNP, there is approximately one G*40*P molecule per 21-nt ssDNA segment. It is probable, therefore, that in the presence of AMP-PNP, there is one G*40*P molecule bound to ssDNA in complex I and two G*40*P molecules in complex II. The binding of two G*40*P molecules to the same ssDNA segment does not seem to be cooperative, because only when all the ssDNA is saturated with one helicase are type II complexes formed.

To understand whether the affinity of G*40*P for a replication fork structure is similar to the affinity of G*40*P for naked ssDNA (i.e. whether G*40*P also interacts with an adjacent dsDNA region), the affinity of G*40*P for a single-arm substrate [a 39-bp duplex with either a 16- or a 25-nt single-arm poly(dA) at the 5′ end (39/16 5′ single-arm and 39/25 5′ single arm), or 3′ end (39/16 3′ single arm or 39/25 3′ single arm)] or a forked substrate [a 39-bp duplex with a double arm of 16-nt or 25-nt poly(dA) (39/16 forked substrate or 39/25 forked substrate)], in the presence of 1 mM AMP-PNP, was assayed. The affinity of G*40*P for the 39/16 5′ single arm or 39/16 forked substrates is ~8-fold lower, when compared with the unstructured 55-nt ssDNA (Fig. 3C). The affinity of G*40*P for the 39/25 5′ single arm or 39/25 forked substrates is ~2.5-fold higher than that for the 39/16 5′ single arm and forked substrates (Fig. 3C) but still >3-fold lower than to the unstructured 55-nt ssDNA. It is probable that the binding site of G*40*P for the 5′-tail ssDNA must be somehow longer than 25 nt. Alternatively, the duplex region of the forked molecule affects the binding to ssDNA. In this respect G*40*P is different from DnaB. Here, the duplex part of the fork does not significantly affect the binding of the enzyme to the ssDNA arm (28).

G*40*P forms only one type of complex with the 39/16 single-arm substrates (Fig. 3D). The affinity of G*40*P to the 39/16 3′ single-arm substrate was 9-fold lower, compared with the affinity of G*40*P for the 39/16 5′ single-arm substrate (Fig. 3C and D), indicating that the duplex region affects the positioning of G*40*P on the single-arm substrate. These results are consistent with the different binding affinity observed by fluorescence for *E.coli* DnaB with 5′ or 3′ single-arm substrates. DnaB accommodates a hexamer in the 20-nt long 3′ tail while another hexamer is associated, in opposite orientation, with the 5′ tail of the fork (28), suggesting that polarity in the binding may be a common feature of all replicative hexameric helicases.

G*40*P preferentially binds to the 5′-tail ssDNA and interacts with duplex DNA

DNA unwinding by the catalytic action of a replicative helicase, with an interconverting population of hexameric rings with a C_6 and C_3 symmetry, requires two ssDNA tails next to the duplex region and involves unidirectional translocation and base pair separation (reviewed in 6,18,19). Several general models (helix destabilising, rolling circle, wedge and torsional) for disruption of the forces that stabilise the duplex have been proposed (reviewed in 6,18,19). In the helix-destabilising model the helicase would bind to the unwinding junction, interact with the duplex DNA, but an interaction with the 3′-ssDNA arm is not obvious. In a type of rolling circle model, the hexamer encircles the 5′ tail and interacts with the 3′ tail and the duplex DNA. In the wedge and torsion models, the hexameric helicase does not interact with the duplex DNA. In the wedge variant the hexameric helicase interacts with the separated strand at the unwinding junction and the excluded 3′ tail does not have a specific interaction

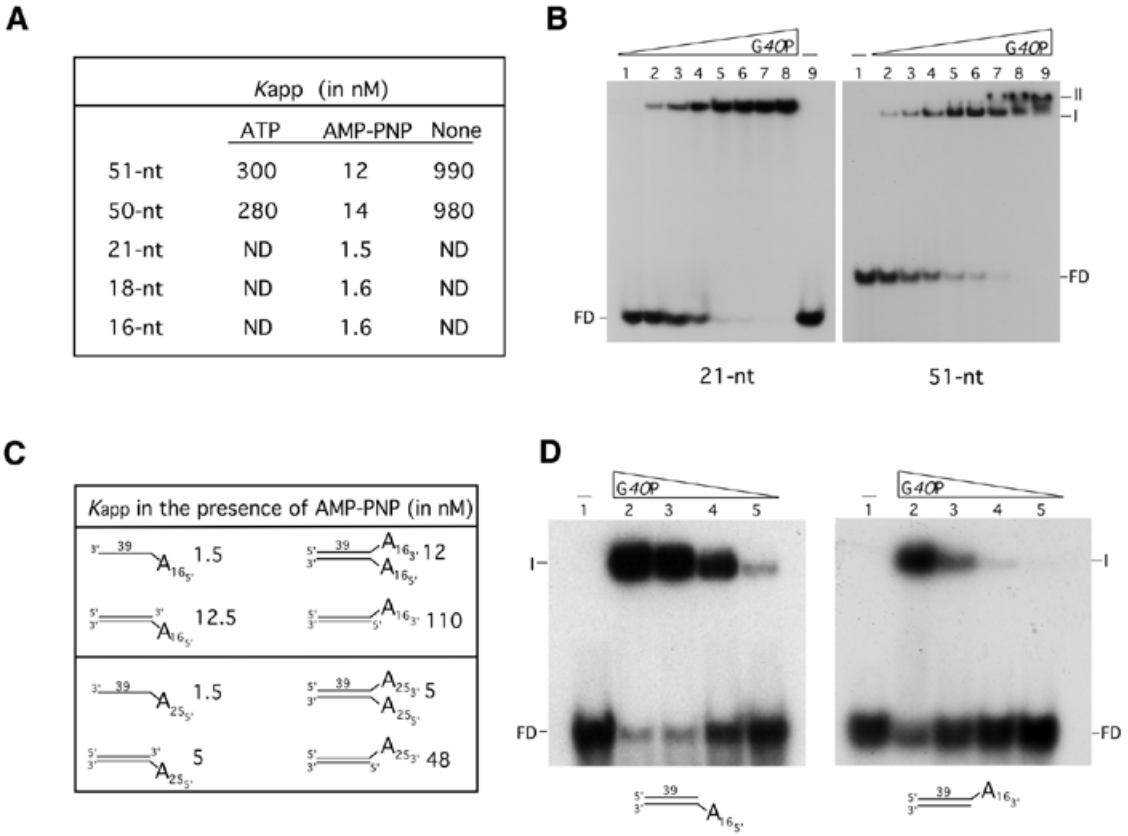

Figure 3. G*40*P–DNA complex formation. (**A**) K_{app} of G*40*P for 51- or 50-nt [γ-^{32}P]ssDNA (2 nM) in the absence or the presence of ATP or AMP-PNP measured by EMSA. The K_{app} of G*40*P for 21-, 18- and 16-nt [γ-^{32}P]ssDNA segments, in the presence of AMP-PNP, were also measured. (**B**) EMSA of G*40*P with a 21-nt [γ-^{32}P]ssDNA (G*40*P concentrations doubling from 0.25 to 32 nM) and with a 51-nt [γ-^{32}P]ssDNA segment (G*40*P concentrations doubling from 3 to 384 nM) were assayed. The two types of complexes obtained are denoted by I and II, and FD denotes the ssDNA in the absence of G*40*P. (**C**) K_{app} of G*40*P for [γ-^{32}P]-single-arm or [γ-^{32}P]-forked substrates in the presence of AMP-PNP, measured by EMSA, are shown. All K_{app} data represent the average of three independent experiments. The poly(dA)$_{16}$ and poly(dA)$_{25}$ regions are denoted as an oblique line. (**D**) EMSA of G*40*P with a 5′ single-arm substrate (G*40*P concentrations doubling from 6 to 50 nM) and with 3′ single-arm substrate (G*40*P concentrations doubling from 25 to 200 nM). The complexes obtained are denoted by I and FD denotes the protein-free DNA.

with the hexameric helicase, whereas in the torsion variant of the model, the hexameric helicase interacts with both tails of the fork.

Previously, it has been shown that the optimal rate of unwinding of forked DNA of hexameric helicases requires a DNA varying from ~8 to 35 nt at the 5′ tail and ~15 to ~30 nt at the 3′ tail (20,29,30). DNA binding affinity experiments suggest that G*40*P has an ~8-fold higher preference for 5′ single-arm substrates than for a 3′ single-arm substrates. To address with which DNA strand G*40*P interacts, we have performed nuclease protection studies using either *Exo*III, *Exo*VI or *Exo*VII in the presence or absence of a non-hydrolysable ATP analogue (e.g. AMP-PNP or ATPγS) and an artificial 39/16 or 39/25 forked substrate with a 16- or 25-nt long tails. As the same results are obtained when 1 mM AMP-PNP or 1 mM ATPγS, or when the 39/16 or 39/25 forked substrate were used, only the former conditions are shown.

The protection of the DNA ends by the binding of G*40*P (12.5 and 25 nM), in the presence or absence of 1 mM AMP-PNP, were performed and the products separated by dPAGE. Protection at the 3′-ssDNA tail from digestion by *Exo*VII was analysed by labelling the 5′ end (top strand, denoted by an asterisk in Fig. 4A) of the duplex. *Exo*VII catalyses exonucleolytic cleavage of ssDNA in either 5′ → 3′ or 3′ → 5′ to yield 5′-phosphomononucleotides. In the presence of AMP-PNP, G*40*P bound to a single region of the forked substrate fails to protect >90% of the 3′-tailed DNA segments from *Exo*VII digestion rendering a 44 ± 2-nt long segment (Fig. 4A). Such effect is independent of the addition of saturating amounts of G*40*P (25 nM, K_{app} ~11 nM). G*40*P in the presence of AMP-PNP only protects a very small fraction of the 3′-tailed DNA segment from *Exo*VII degradation. This is consistent with the fact that at these G*40*P concentrations, there is little binding of G*40*P to the 3′ arm (K_{app} 110 nM; see Fig. 3C). Furthermore, we could rule out a low 'strength' of the *Exo*VII when attacking the 3′ arm, because when a G*40*P mutant was assayed, the 3′-arm substrate is fully protected from *Exo*VII degradation (data not shown).

The protection at the 5′-ssDNA tail was then analysed by labelling the 3′ end (bottom strand, denoted by an asterisk in Fig. 4B) of the duplex. In the absence of AMP-PNP, there is no binding of G*40*P to ssDNA hence the fork is sensitive to *Exo*VII digestion rendering a 44 ± 2-nt long labelled segment, whereas in the presence AMP-PNP G*40*P fully protects the

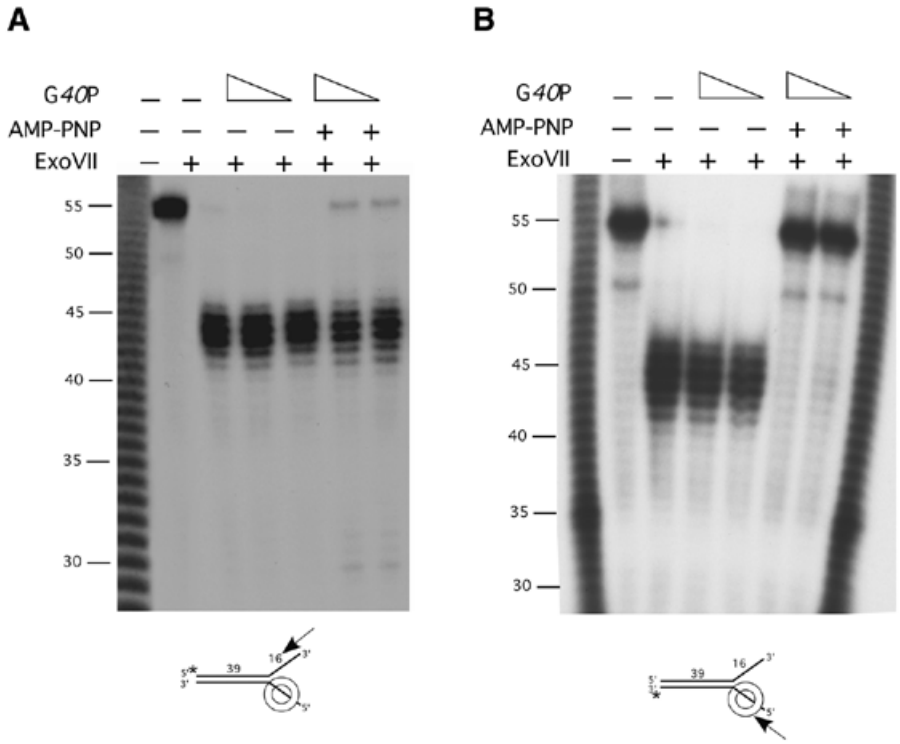

Figure 4. G*40*P protection of the ssDNA arms of a forked molecule. G*40*P (12.5 and 25 nM) was incubated with 2 nM of double-arm substrate labelled at the 5′ end (**A**) or at the 3′ end (**B**) of the duplex in the presence or in the absence of 1 mM AMP-PNP. After 15 min incubation at 37°C, *Exo*VII (0.2 U) was added and the incubation was continued for 15 min at 37°C. The digestions were stopped and samples separated by 10% dPAGE and analysed by autoradiography. G*40*P encircling the 5′ tail of the 39/16 forked substrate is depicted not at scale. The symbols + and – denote the presence or absence of the indicated product. The asterisk denotes the labelled end. The arrow indicates the direction of exonucleolytic digestion. [γ-^{32}P]poly(dA) is used as a 1-nt molecular weight ladder.

ssDNA segment of exonucleolytic attack (Fig. 4B). Similar results were obtained with the 39-bp duplex containing a 25-nt long [poly(dA)] double arm, indicating that although the affinity of G*40*P for forked molecules having short (16 nt) tails is ~2-fold lower (see Fig. 3C), it is positioned in the same manner in the 39/16 and in the 39/25 forked molecules. It is likely therefore that G*40*P binds ssDNA with a 5′ → 3′ orientation with respect to the polarity of the ssDNA sugar–phosphate backbone. This is consistent with the differences in K_{app} observed for a single-arm substrate with a 5′ or 3′ tail (Fig. 3C), with the findings of EM studies for the T7 gp4 helicase (31), or with fluorescence studies for DnaB (27). We show that at the concentrations used, G*40*P interacts with the 5′ tail, but is unable to encircle or even interact with the 3′-tail region of a forked DNA substrate. This is consistent with the observation that the K_{app} is similar for the 5′ single-arm substrate and for the forked substrate, but ~9-fold lower for the for the 3′ single-arm substrate (Fig. 3C). It is also consistent with other indirect data described, such as that the *Thermus aquaticus* DnaB unwinds forked-duplex DNA with a similar rate when the 3′ tail has a reversed polarity (32), or as that streptavidin, bound to the 3′ end of the duplex, fully substitutes for the 3′-ssDNA tail in T7 gp4 helicase activity (30).

The protection at the 5′ dsDNA from digestion by *Exo*VI was analysed by labelling the 3′-ssDNA end (top strand denoted by an asterisk in Fig. 5A). *Exo*VI catalyses in a stepwise non-processive reaction removal of 5′-phosphomononucleotides from the 5′ termini of dsDNA. In the absence of AMP-PNP, no protection of the duplex was observed, because digestion with *Exo*VI renders a 26 ± 3-nt long labelled segment in the presence or absence of G*40*P (Fig. 5A). Perhaps due to poor stability of the short duplex (15), complete digestion by *Exo*VI was not observed and ~10 bp from the duplex became resistant to degradation. In the presence of AMP-PNP, a labelled 32 ± 2-nt segment, indicative of a G*40*P protection of the duplex ~15 bp away from the junction was observed, which could not be degraded by using the double amount of *Exo*VI (Fig. 5A). The protection at the 3′ dsDNA from digestion by *Exo*III was then analysed by labelling the 5′-ssDNA end (bottom strand, Fig. 5B). *Exo*III catalyses the stepwise removal of 5′-phosphomononucleotides from the 3′-OH termini of blunt or 3′ recessed dsDNA, but 3′ overhangs >4 nt are protected from *Exo*III digestion. In the absence of AMP-PNP, protection of *Exo*III digestion renders 24 ± 1-nt long labelled segment (Fig. 5B). A complete digestion of the duplex by *Exo*III was not observed and ~8 bp became resistant to degradation. This has also been observed by other authors (15) and suggests again a poor stability of the duplex. In the presence of AMP-PNP, a labelled segment of ~25 ± 1 nt indicative of a protection of the duplex ~9 bp away from the junction by G*40*P was observed, which could not be degraded by using the double amount of *Exo*III (Fig. 5B). The dependence of the protection caused by G*40*P in the duplex region on AMP-PNP indicated that G*40*P did not bind directly to the dsDNA, since binding to dsDNA is independent of AMP-PNP (25). We might envisage that the protection of the duplex is due to initial binding of G*40*P to

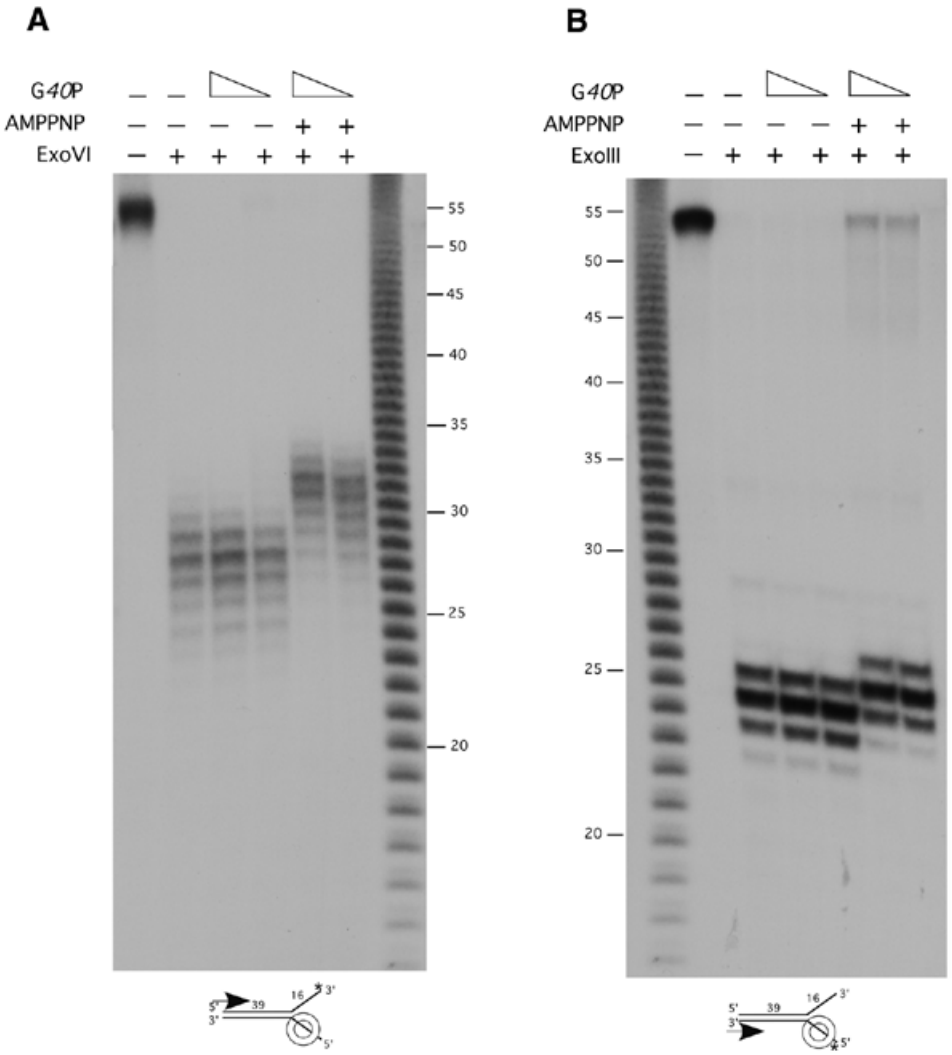

Figure 5. G*40*P protection of the duplex region of the 39/16 forked molecule. G*40*P (12.5 and 25 nM) was incubated with 2 nM of forked molecule labelled at the 3′ (**A**) or at the 5′ end (**B**) of the ssDNA tail, in the presence or in the absence of 1 mM AMP-PNP. After 15 min incubation a 37°C, *Exo*VI (1 U) (A) or *Exo*III (1 U) (B) was added and the incubation was continued for 15 min at 37°C. The digestions were stopped and samples separated by 15% dPAGE and analysed by autoradiography. G*40*P encircling the 5′ tail of the 39/16 forked substrate is depicted not at scale. The symbols + and – denote the presence or absence of the indicated product. The asterisk denotes the labelled end. The arrow indicates the direction of exonucleolytic digestion. [γ-^{32}P]poly(dA) is used as a 1-nt molecular weight ladder.

ssDNA and then to the adjacent duplex junction. Alternatively, a destabilisation of the duplex is due to initial binding of G*40*P to ssDNA with a subsequent 'breathing' of the ss/dsDNA junction by distorting the structure of the encircled tail as proposed previously by Yu *et al.* (33). To discriminate between these two options we performed $KMnO_4$ footprinting on both strands using the 39/16 or 39/25 forked molecule, labelled at the 5′ end. The $KMnO_4$ footprinting pattern in the presence of both AMP-PNP and G*40*P (25 nM) is indistinguishable from that in the absence of G*40*P, hence we favoured the model in which G*40*P interacts asymmetrically with the 'fork DNA', is bound to the 5′ tail, and contacts the duplex region of both strands. No breathing of the ss/dsDNA junction could be observed by $KMnO_4$ footprinting by using a forked substrate having an AT-rich segment at the junction region (data not shown). G*40*P seems to make a more extent contact with the duplex region of the strand opposite to where G*40*P is bound. Furthermore, G*40*P does not seem to interact with the 3′ tail. These results are not consistent with the rolling circle, wedge and torsional model of DNA unwinding (6).

The G*40*P central channel binds ssDNA

Hexameric replicative DNA helicases have a central channel with a diameter of 25–45 Å that could accommodate a dsDNA or a ssDNA (reviewed in 6,18,19). No G*40*P protection on the 3′-ssDNA arm and full protection on the 5′-ssDNA arm (Fig. 4) suggests that the 5′-end ssDNA might have entered the central channel of G*40*P whereas the 3′-end ssDNA might be excluded. We cannot exclude a wrapping of the 5′-ssDNA arm around G*40*P from our studies, but we find it unlikely that a small 16-nt long ssDNA tail can be occluded from exonuclease digestion by wrapping around a G*40*P monomer. To address whether the ssDNA occupies the central channel of G*40*P, electron microscopic analysis was performed. Protein-free

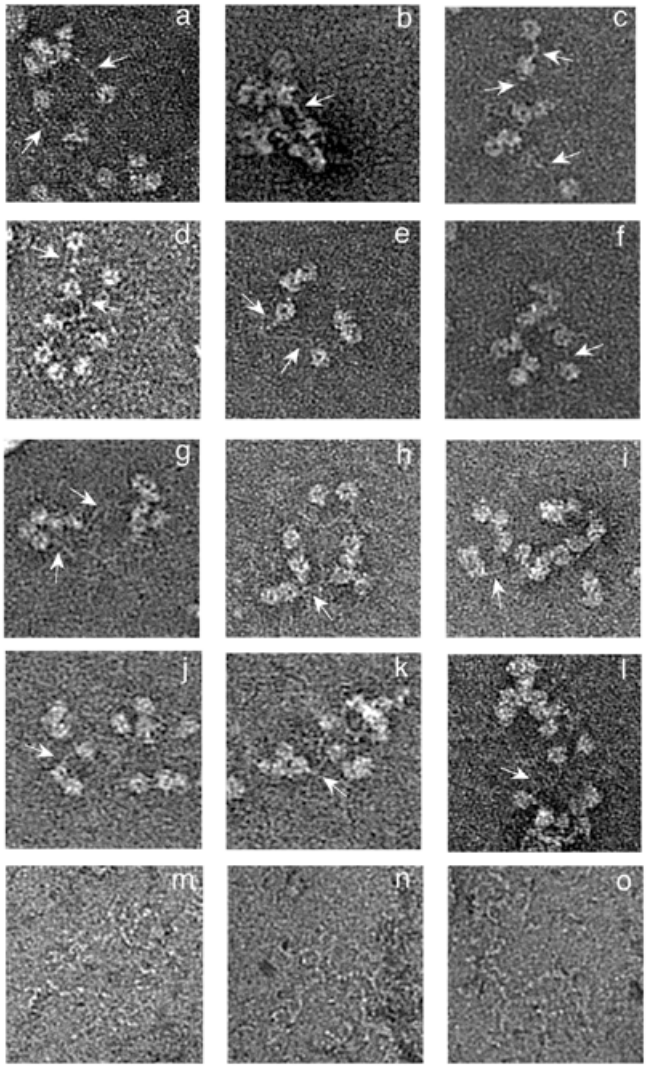

Figure 6. Electron micrographs of G*40*P bound to viral M13mp18 DNA in the presence of AMP-PNP. ssM13mp18 DNA (0.2 nM) was incubated, in buffer C, with G*40*P (50 nM) during 15 min at 37°C, and the complexes were visualised by EM. The regions of ssDNA entering the G*40*P inner channel are denoted by arrows (**a–l**). Three controls of ssM13mp18 in the absence of G*40*P are shown in (**m–o**).

ssDNA is at the visualisation limit of electron microscopy, but the addition of single-stranded DNA binding (SSB) protein to visualise the ssDNA will obscure the view in our case, because SSB exert a negative effect in G*40*P–AMP-PNP interaction with ssDNA (4).

The thin filament of ssDNA might bind along the circumference or in the centre of the G*40*P hexameric ring. Binding along the circumference would require tangential approach of ssDNA to the G*40*P ring, whereas the binding in the centre would result in an approach that is along the radius of the G*40*P ring. In the images, where the circular ssDNA could be visualised, a perpendicular approach of ssDNA to the circumference of the G*40*P–AMP-PNP hexameric ring is observed (Fig. 6). These results support the proposal that ssDNA binding is in the centre of the G*40*P ring. This is consistent with other indirect observations reported for DnaB, T4 gp41 and T7 gp4, which

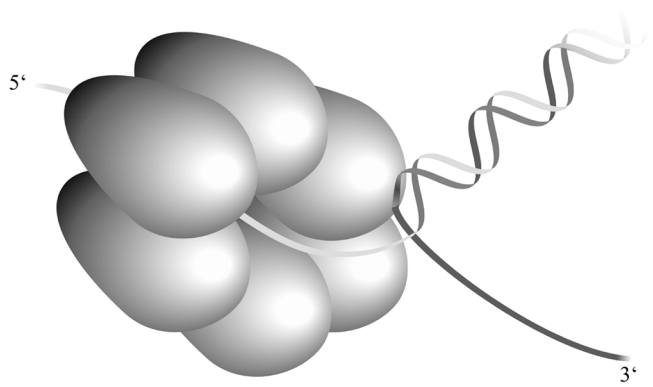

Figure 7. Proposed model of unwinding of DNA by G*40*P. G*40*P binds ssDNA in a 5′ → 3′ polarity through the inner channel, contacting the 5′-ssDNA arm, whereas there is no interaction with the 3′ arm which is fully excluded. G*40*P interacts with dsDNA at the junction. Protein conformational changes and ATP hydrolysis would lead to base pair separation. Then, the hexamer would translocate and bind to the newly separated stretch of the strand.

suggest that replicative helicases bind ssDNA through the central channel (reviewed in 6,19), and argue against a wrapping of the ssDNA around G*40*P.

Although the precise mechanism of DNA unwinding is not known, we assume that the different G*40*P conformational states and the coupling of ssDNA binding and ATP hydrolysis may be the driving force to melt the duplex DNA and propel the helicase forward along the ssDNA strand. This is consistent with the fact that we did not observe any difference in the $KMnO_4$ footprint with G*40*P in the presence of the non-hydrolysable ATP analogue AMP-PNP.

As illustrated in Figure 7, on an artificial substrate, G*40*P binds to the 5′ arm of a forked molecule and encircles it in an NTP-dependent fashion while it fully excludes the 3′ arm. G*40*P makes a contact with both strands of the dsDNA at the junction, and this contact is more extended with the strand to which G*40*P is not bound. At least 5 nt are protected in this strand from *Exo*VI attack, whereas only 1 nt is protected from *Exo*III digestion in the dsDNA region adjacent to the 5′-ssDNA arm to which G*40*P is bound. The fact that (i) only one of the six subunits of ATP-activated helicase appears to be in close contact with the ssDNA (27,28, our unpublished results) and that (ii) the helicase dissociates from the DNA upon ATP hydrolysis, favours a mechanism in which a monomer participates in the ssDNA binding and release. The contact with dsDNA could arise as the consequence of the fact that the ring is specifically positioned just at the junction. Only the hydrolysis of the NTP produces helicase movement and unwinding of the DNA in a 5′ → 3′ direction.

ACKNOWLEDGEMENTS

This research was partially supported by grants BMC2000-0548 and SAF2001-4339 from MCyT-DGI and QLK2-CT-2000-00634 from the European Union to J.C.A., 31-58841.99 from Swiss National Science Foundation to J. Dubochet and A.S. and from Human Frontier Science Program to A.S. We are very grateful

to T. A. Trautner and J. Dubochet for their interest in this project.

REFERENCES

1. Pedré,X., Weise,F., Chai,S., Lüder,G. and Alonso,J.C. (1994) Characterization of *cis* and *trans* acting elements required for the initiation of DNA replication in the *Bacillus subtilis* bacteriophage SPP1. *J. Mol. Biol.*, **236**, 1324–1340.
2. Missich,R., Weise,F., Chai,S., Lurz,R., Pedré,X. and Alonso,J.C. (1997) The replisome organizer (G*38*P) of *Bacillus subtilis* bacteriophage SPP1 forms specialized nucleoprotein complexes with two discrete distant regions of the SPP1 genome. *J. Mol. Biol.*, **270**, 50–64.
3. Ayora,S., Stasiak,A. and Alonso,J.C. (1999) The *Bacillus subtilis* bacteriophage SPP1 G*39*P delivers and activates the G*40*P DNA helicase upon interacting with the G*38*P-bound replication origin. *J. Mol. Biol.*, **288**, 71–85.
4. Ayora,S., Langer,U. and Alonso,J.C. (1998) *Bacillus subtilis* DnaG primase stabilises the bacteriophage SPP1 G*40*P helicase-ssDNA complex. *FEBS Lett.*, **439**, 59–62.
5. Bárcena,M., San Martin,C., Weise,F., Ayora,S., Alonso,J.C. and Carazo,J.M. (1998) Polymorphic quaternary organization of the *Bacillus subtilis* bacteriophage SPP1 replicative helicase (G*40*P). *J. Mol. Biol.*, **283**, 809–819.
6. Patel,S.S. and Picha,K.M. (2000) Structure and function of hexameric helicases. *Annu. Rev. Biochem.*, **69**, 651–697.
7. San Martín,M.C., Stamford,N.P., Dammevora,N., Dixon,N.E. and Carazo,J.M. (1995) A structural model for the *Escherichia coli* DnaB helicase based on electron microscopy data. *J. Struct. Biol.*, **114**, 167–176.
8. Yu,X., Jezewska,M.J., Bujalowski,W. and Egelman,E.H. (1996) The hexameric *E.coli* DnaB helicase can exist in different quaternary states. *J. Mol. Biol.*, **259**, 7–14.
9. Yanisch-Perron,C., Vieira,J. and Messing,J. (1985) Improved M13 phage cloning vectors and host strains: nucleotide sequences of the M13mp18 and pUC19 vectors. *Gene*, **33**, 103–119.
10. Studier,F.W. (1991) Use of bacteriophage T7 lysozyme to improve an inducible T7 expression system. *J. Mol. Biol.*, **219**, 37–44.
11. Sambrook,J., Fritsch,E.F. and Maniatis,T. (1989) *Molecular Cloning. A Laboratory Manual*, Vol. 1–3. Cold Spring Harbor Laboratory Press, Cold Spring Harbor, NY.
12. Ayora,S., Rojo,F., Ogasawara,N., Nakai,S. and Alonso,J.C. (1996) The Mfd protein of *Bacillus subtilis* 168 is involved in both transcription-coupled DNA repair and DNA recombination. *J. Mol. Biol.*, **256**, 301–318.
13. Gill,S.C. and von Hippel,P.H. (1989) Calculation of protein extinction coefficient from amino acid sequence data. *Anal. Biochem.*, **182**, 319–326.
14. Scott,J.F., Eisenberg,S., Bertsch,L. and Kornberg,A. (1977) A mechanism of duplex DNA replication revealed by enzymatic studies of phage phi X174: catalytic strand separation in advance of replication. *Proc. Natl Acad. Sci. USA*, **74**, 193–197.
15. Soultanas,P., Dillingham,M.S., Wiley,P., Webb,M.R. and Wigley,D.B. (2000) Uncoupling DNA translocation and helicase activity in PcrA: direct evidence for an active mechanism. *EMBO J.*, **19**, 3799–3810.
16. Sogo,J., Stasiak,A., DeBernardin,W., Losa,R. and Koller,Th. (1987) Binding of proteins to nucleic acids as studied by electron microscopy. In Sommerville,J. and Scheer,U. (eds), *Electron Microscopy in Molecular Biology*. IRL Press, Oxford, UK, pp. 61–79.
17. Bird,L.E., Pan,H., Soultanas,P. and Wigley,D.B. (2000) Mapping protein–protein interactions within a stable complex of DNA primase and DnaB helicase from *Bacillus stearothermophilus*. *Biochemistry*, **39**, 171–182.
18. Lohman,T.M. and Bjornson,K.P. (1996) Mechanisms of helicase-catalyzed DNA unwinding. *Annu. Rev. Biochem.*, **65**, 169–214.
19. Soultanas,P. and Wigley,D.B. (2001) Unwinding the 'Gordian knot' of helicase action. *Trends Biochem. Sci.*, **26**, 47–54.
20. Arai,K.I and Kornberg,A. (1981) Mechanism of *dna*B protein action. Allosteric role of ATP in the alteration of DNA structure by *dna*B protein in priming replication. *J. Biol. Chem.*, **256**, 5260–5266
21. Liu,C.C. and Alberts,B.M. (1981) Characterization of the DNA-dependent GTPase activity of T4 gene 41 protein, an essential component of the T4 bacteriophage DNA replication apparatus. *J. Biol. Chem.*, **256**, 2813–2820.
22. Venkatesan,M., Silver,L.L. and Nossal,N.G. (1982) Bacteriophage T4 gene 41 protein, required for the synthesis of RNA primers, is also a DNA helicase. *J. Biol. Chem.*, **257**, 12426–12434.
23. Matson,S.W. and Richardson,C.C. (1983) DNA-dependent nucleoside 5′-triphosphatase activity of the gene 4 protein of bacteriophage T7. *J. Biol. Chem.*, **258**, 14009–14016.
24. Hingorani,M.M. and Patel,S.S. (1993) Interactions of bacteriophage T7 DNA primase/helicase protein with single-stranded and double-stranded DNAs. *Biochemistry*, **32**, 12478–12487.
25. Weise,F. (1997) Biochemische Charakterisierung der Initiation der DNA-Replikation des *Bacillus subtilis*-Bakteriophagen SPP1. Dissertation thesis, Freie Universität Berlin, Germany.
26. Bujalowski,W. and Jezewska,M.J. (1995) Interactions of *Escherichia coli* primary replicative helicase DnaB protein with single-stranded DNA. The nucleic acid does not wrap around the protein hexamer. *Biochemistry*, **34**, 8513–8519.
27. Jezewska,M.J., Rajendran,S. and Bujalowski,W. (1998) Functional and structural heterogeneity of the DNA binding of the *Escherichia coli* primary replicative helicase DnaB protein. *J. Biol. Chem.*, **273**, 9058–9069.
28. Jezewska,M.J., Rajendran,S. and Bujalowski,W. (1998) Complex of *Escherichia coli* primary replicative helicase DnaB protein with a replication fork. Recognition and structure. *Biochemistry*, **37**, 3116–3136.
29. Ahnert,P. and Patel,S. (1997) Asymmetric interactions of hexameric bacteriophage T7 DNA helicase with the 50 and 30-tails of the forked DNA substrate. *J. Biol. Chem.*, **272**, 32267–32273.
30. Hacker,K.J. and Johnson,K.A. (1997) A hexameric helicase encircles one DNA strand and excludes the other during DNA unwinding. *Biochemistry*, **36**, 14080–14087.
31. Egelman,E.H., Yu,X., Wild,R., Hingorani,M. and Patel,S.S. (1995) Bacteriophage T7 helicase/primase proteins form rings around single-stranded DNA that suggest a general structure for hexameric helicases. *Proc. Natl Acad. Sci. USA*, **92**, 3869–3873.
32. Kaplan,D.L. (2000) The 3′-tail of a forked-duplex sterically determines whether one or two DNA strands pass through the central channel of a replication-fork helicase. *J. Mol. Biol.*, **301**, 285–299.
33. Yu,X., Hingorani,M.M., Patel,S.S. and Egelman,E.H. (1996) DNA is bound within the central hole to one or two of the six subunits of the T7 DNA helicase. *Nature Struct. Biol.*, **3**, 740–743.